Nanoscale Surface Activation via Reticular Chemistry for Reactive H_2S Sequestration Surpassing 1500 mg_{H2S} g^{-1} under Ambient Conditions

*Li Shiuan Ng[a]‡, Jun Jing Teh[a]‡, Zhi Zhong Ang[a], Veronica Pereira[a], Sankar Das[a], Brynne Shu Ni Tan[a], Hiang Kwee Lee[a], [b], [c]**

[a] Division of Chemistry and Biological Chemistry, School of Chemistry, Chemical Engineering and Biotechnology, Nanyang Technological University, 21 Nanyang Link, Singapore 637371 Singapore.

[b] Institute of Materials Research and Engineering, The Agency for Science, Technology and Research (A*STAR), 2 Fusionopolis Way, #08-03, Innovis, Singapore 138634 Singapore.

[c] Centre for Hydrogen Innovations, National University of Singapore, E8, 1 Engineering Drive 3, Singapore 117580 Singapore.

‡These authors contribute equally to this work.

*Correspondence to: hiangkwee@ntu.edu.sg

Keywords: hydrogen sulfide • interfacial reaction • metal organic framework • surface activation • reticular chemistry

Abstract

Efficient H_2S removal from industrial emissions and the environment is crucial for safeguarding human health and ecosystems. Conventional metal oxide-based materials for H_2S sequestration trap sulfur species in solid matrices but suffer from low uptake capacity (<65 $mg_{H2S}{\cdot}g^{-1}$) and require elevated operating conditions due to limited active sites and kinetic barriers. Herein, we achieve efficient H_2S sequestration at ambient conditions by chemically activating metal oxide surfaces using reticular chemistry to enhance solid-gas reactions. This approach integrates metal oxide core with a metal-organic framework (MOF) layer, forming a surface-activated interfacial nanoreactor (SAIN). The MOF facilitates H_2S transfer to the functional interface while activating the metal oxide surface for enhanced reactivity. SAIN achieves higher H_2S sequestration of up to 1524 $mg_{H2S}{\cdot}g^{-1}$ across a wide concentration range with nearly 100% efficiency. It demonstrates a >23-fold improvement over standalone metal oxide and/or MOF platforms and higher than emerging materials by up to 508-fold in H_2S uptake and 24-fold in sequestration rate. Mechanistic studies reveal that interfacial electron migration and electronic hybridization weaken metal-oxygen bonds, enhancing their interactions with H_2S and promoting efficient reactive sequestration. Our “activate-react-lock” strategy offers valuable insights for designing functional interfaces to activate nanomaterial surfaces for diverse environmental, chemical, and energy applications.

Introduction

Mitigating hydrogen sulfide (H_2S) emissions is critical due to its serious health and environmental risks.[1-3] H_2S causes olfactory paralysis above 100 ppm, rendering it undetectable without specialized instruments, while concentrations over 1000 ppm can cause instant death and levels as low as 5 ppm trigger respiratory irritation.[4, 5] Consequently, regulatory agencies have set 100 ppm as the "immediately dangerous to life and health" (IDLH) limit and 10 ppm as the recommended exposure limit (REL).[6] Environmentally, H_2S contributes to the acidification of water bodies, soil degradation, and ecosystem breakdown.[7] H_2S emissions are prevalent in industries such as chemical production, energy, maritime, and waste treatment, where concentrations range from a few ppm to over 1000 ppm.[8-10] Conventional H_2S removal methods rely on liquid-based scrubbing systems, which use alkaline solutions or ionic liquids to neutralize H_2S into less toxic sulfur species.[11-13] However, these methods suffer from poor gas-to-liquid transfer efficiency and difficulty maintaining solution alkalinity, particularly under high H_2S loads or prolonged use. They also struggle to capture H_2S at low concentrations, making it challenging to meet industrial needs. Additionally, dissolved H_2S poses downstream pollution risks, as soluble sulfur species (*e.g.*, sulfides, thiosulfate, sulfate) remain hazardous and generate toxic liquid waste that requires further treatment.[14]

Solid-based materials offer a promising solution to overcome the inefficiencies of gas-to-liquid transfer and reduce secondary pollution by enabling direct gas-solid interactions through two main mechanisms, namely (1) adsorption and (2) chemical reaction.[13, 15] Adsorbents (*e.g.*, zeolites, activated carbon) have been widely explored for H_2S capture, but their reliance on weak non-covalent interactions leads to low adsorption capacity at ambient conditions and susceptibility to desorption when exposed to competing gases or elevated temperatures.[16, 17]

Metal-organic frameworks (MOFs) are emerging adsorbent materials owing to their highly tunable porosity, large surface area, and gas permeability, making them suitable for various gas application.[18-20] However, their current studies on H_2S adsorption are typically measured under high pressure conditions (1.6 MPa) with isotherm studies. In contrast, metal oxides (*e.g.*, MnO) sequester H_2S by forming strong metal-sulfide bonds through solid-gas reactions.[21] However, the high temperatures required for these reactions (400-1000 ºC) limit their broader applicability due to high energy demands and potential sublimation of metal oxides at these temperatures.[22] To enhance desulfurization at ambient conditions, recent research has focused on developing hybrid materials by integrating metal oxides with other materials to improve reactivity.[5] For instance, Mn_2O_3/Fe_2O_3 hybrid has demonstrated improved H_2S sequestration (12 mg_{H2S} g^{-1}) via an adsorption-oxidation mechanism which is higher than their individual components.[23] However, these systems still face formidable challenges such as low uptake (<65 mg_{H2S} g^{-1}), slow reaction rates (up to 24 hours), and the need for elevated operating conditions (*e.g.*, up to 550 ºC and 16 atm).[20, 24, 25] These limitations arise from the limited number of active sites and poor reactivity due to kinetic barriers, especially under ambient conditions. Furthermore, the formation of metal sulfates during H_2S sequestration introduces leaching risks in aqueous environments due to their high solubility, potentially leading to environmental contamination.[23] Thus, developing new strategies to enhance H_2S sequestration, even at low concentrations and under ambient conditions, is vital for mitigating the hazardous effects of this toxic gas.

Herein, we achieve efficient H_2S sequestration under ambient conditions by leveraging a multifunctional interface formed between a metal oxide and a metal-organic framework (MOF) to boost solid-gas reactions. This approach integrates two key concepts. (1) The MOF coating serves as a porous scaffold with high H_2S adsorptivity, enabling direct H_2S capture from the gas

phase and facilitating its transfer to the metal oxide. Additionally, the MOF's metal nodes and organic linkers interact with the metal oxide, promoting synergy at the interface. (2) We exploit interfacial chemical interactions to promote electron density migration and frontier orbital mixing at the point of interaction, thereby activating the metal oxide surface. This surface activation drives the reactive entrapment of H_2S to produce insoluble MnS. Our surface-activated interfacial nanoreactor (SAIN) design uniquely enhances the intrinsic reactivity of materials, setting it apart from conventional approaches that primarily focus on increasing adsorption sites in porous and hybrid materials.

As a proof-of-concept, SAIN demonstrates efficient and rapid (~1 h) gas-phase H_2S sequestration, achieving up to 1524 mg_{H2S} g^{-1} and effective gas sequestration across a wide concentration range, including ~100% sequestration efficiency at concentration levels as low as 5 ppm. This performance is >23-fold higher than control platforms using standalone metal oxide and/or MOF components, underscoring the unique reactivity of the interfacial nanoreactor that is unattainable with individual materials or their physical mixtures. SAIN also demonstrate higher performance over other emerging designs by up to 508-fold in maximal H_2S uptake and 24-fold in sequestration rate compared to trsuperiansition metal oxides, MOFs, and their hybrids. Moreover, SAIN functions as an effective sulfur trap by forming insoluble metal sulfide as the primary product, preventing leaching in both simulated and real-world water samples. Simulation and experimental studies reveal that this enhanced surface activation arises from electron re-distribution and electronic modulation upon hybrid formation, which weakens the metal-O bond and promotes interaction with H_2S to accelerate the oxygen-to-sulfur exchange. By harnessing reticular chemistry to induce interfacial chemical and electronic hybridization, this work offers valuable insights into activating materials with poor intrinsic reactivity at ambient

conditions, paving the way for new opportunities in solid-gas reactions for environmental, chemical, and energy applications.

Results and Discussion

Synthesis and characterization of SAIN

Our SAIN design leverages on the functional interface between a metal oxide core and a thin MOF coating to efficiently capture H_2S within a solid matrix (Figure 1A). We select MnO as the metal oxide core due to its ability to form stable MnS upon reacting with H_2S, its high natural abundance, and its relatively low toxicity. For the MOF component, we use Materials Institute of Lavoisier-53(Al) (MIL) because of its strong affinity for H_2S gas and its ability to facilitate gas diffusion through its nanoporous structure. We synthesize MnO nanospheres using a thermal decomposition method under an inert atmosphere, yielding particles with a roughened surface and an average diameter of (149 ± 23) nm (Figure S1). The roughened surface increases the available surface area, thereby enhancing interactions with H_2S. Next, we coat the MnO nanospheres with a MIL layer through a wet immersion method. The resulting MnO@MIL nanohybrids retain the roughened surface morphology and exhibit a larger diameter of (158 ± 15) nm, indicating a MIL coating thickness of <20 nm (Figure 1B; Figure S2). In addition, scanning electron microscopy and energy-dispersive X-ray spectroscopy (SEM-EDX) confirm the successful deposition of the MIL layer on the MnO nanosphere surface (Figure S3). Both MnO and MnO@MIL display characteristic MnO diffraction patterns (Figure 1C, Figure S4) corresponding to the Mn(II) oxidation state (PDF #04-013-0265). The unique diffraction patterns of MnO and Mn 3s X-ray photoelectron spectroscopy (XPS) spectra (ΔE = 5.9 eV, indicating Mn^{2+}; Figure 1D; Figure S5) evidently demonstrates that the Mn(II) oxidation state is preserved after hybrid formation. The formation of the MIL coating is further supported by the presence of Al 2p (~74.6 eV) and O 1s (~ 531.4 eV) XPS features that are consistent with pristine MIL. The BET surface area of MnO@MIL, MnO, and MIL are 26 m^2 g^{-1}, 16 m^2 g^{-1}, and 166 m^2 g^{-1},

respectively, where an ultrathin MOF coating increases the surface area of the ensemble (Figure S6). Moreover, the pore diameters of MnO@MIL, MnO, and MIL are similar at 3.64 nm, 3.62 nm and 3.65 nm, respectively, which are ~10-fold larger than the kinetic diameter of H_2S (0.36 nm). Such substantial size difference ensures that the MIL layer allows H_2S molecules to freely permeate through the porous framework and access the activated MnO sites. Moreover, the surface -OH groups on MIL readily interact with the polar H_2S molecules to selectively facilitate its diffusion while exclude the other interference gases. These two attributes jointly facilitate the selective and continuous access of H_2S to the embedded functional interface for efficient sequestration application.

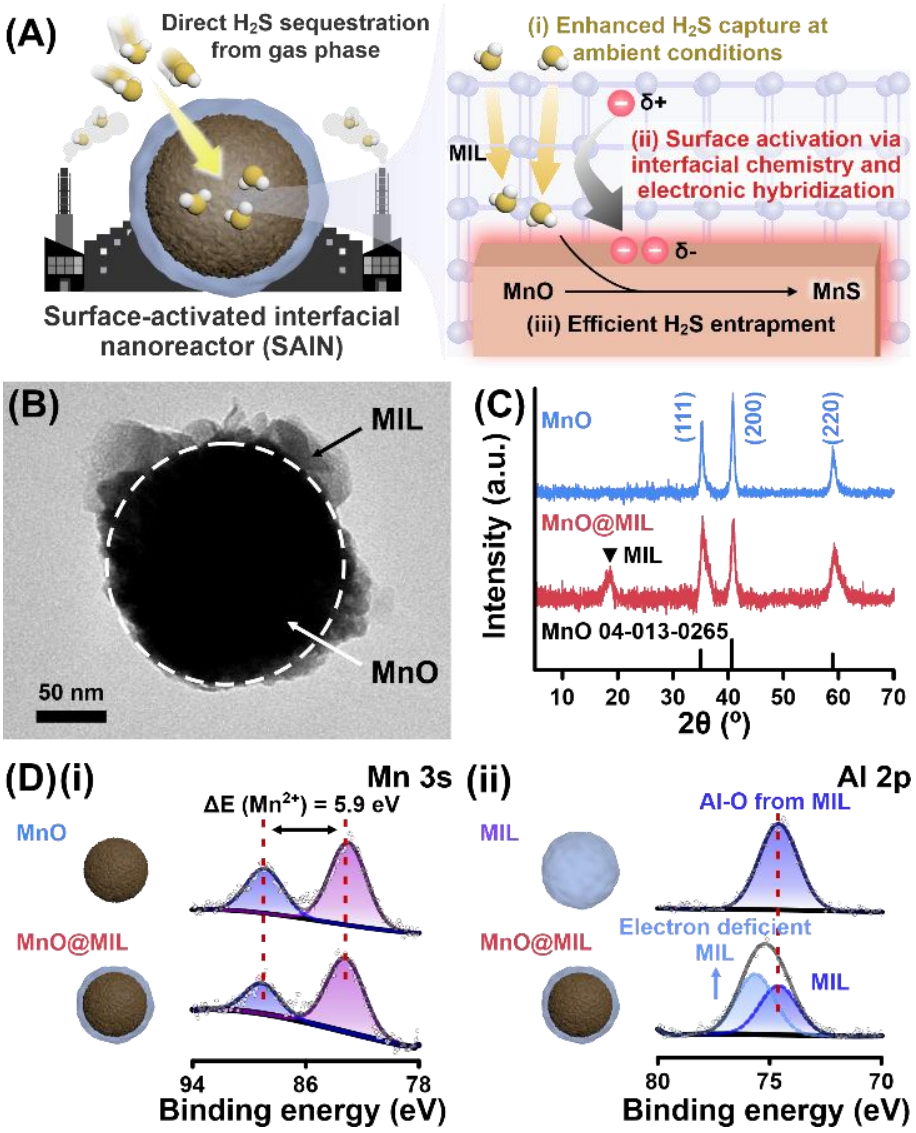


Figure 1. Synthesis and characterization of SAIN. (A) Schematic illustration of the SAIN built on a MnO@MIL design for the effective total sequestration of hydrogen sulfide (H_2S) directly from the gas phase at ambient conditions. (B) Transmission electron microscopy (TEM) image of as-synthesized MnO@MIL. (C) XRD patterns of as-synthesized MnO and MnO@MIL nanohybrid. (D) High-resolution (i) Mn 3s and (ii) Al 2p XPS spectra of MnO nanospheres before and after MIL coating.

We investigate the interfacial chemical microenvironment within the MnO@MIL ensemble using XPS characterization, as the interface is the point-of-reaction and plays a crucial role in promoting material reactivity. High-resolution XPS spectra of O 1s and Al 2p reveal notable changes upon hybrid formation. In the Al 2p spectra, a new peak emerges at a higher binding energy of 75.6 eV in MnO@MIL, compared to ~74.6 eV in pristine MIL (Figure 1D-ii). Additionally, the O 1s spectrum shows a new MIL feature at 532.6 eV, which appears at a higher binding energy than in pristine MIL (531.4 eV; Figure S5). These shifts in binding energy indicate that MIL becomes partially electron-deficient in the nanohybrid. Moreover, we observe a new Mn-O feature in the O 1s XPS spectrum at a lower binding energy of 527.8 eV compared to pristine MnO (529.0 eV and 530.6 eV), signifying that MnO becomes more electron-rich after MIL coating. Two key insights arise from these XPS observations (Figure S7). First, the chemical linkage between MnO and MIL is likely mediated through a MnO-Al bond, as no significant changes are observed in the Mn 2p and Mn 3s XPS spectra. This linkage is essential for facilitating frontier orbital mixing between the two materials. Second, the interfacial interactions drive electron density migration from MIL to MnO, as evident from the simultaneous presence of electron-richer MnO and electron-deficient MIL in MnO@MIL. This MIL-to-MnO electron migration likely localizes onto the oxygen atom of MnO, given the absence of apparent chemical shifts in Mn 2p and Mn 3s XPS spectra of post-hybrid formation. Characterization using ultraviolet photoelectron spectroscopy (UPS) further supports the XPS findings, where MnO@MIL exhibits smaller work function ($\Phi = 3.52 \pm 0.12$ eV) than MnO ($\Phi = 4.36 \pm 0.12$ eV; Figure S8). The work function of a material reflects the minimum energy required for electrons to escape the material, whereby a smaller work function indicates the increase in free electron density in MnO@MIL. These electron re-distribution phenomena and

interfacial chemical hybridization are critical for activating the metal oxide surface for subsequent H_2S sequestration.

Investigation on the H_2S sequestration performance

Prior to applying MnO@MIL for H_2S sequestration, we construct a H_2S-generation chamber and assess its performance by tracking time-dependent H_2S generation (Figure S9). It is noteworthy that this H_2S-generation chamber will be used to control H_2S concentration in the gas stream for subsequent sequestration studies. To ensure complete and accurate detection, two base traps containing aqueous NaOH solution (0.015 M) are used to capture H_2S molecules from the continuous gas stream. The *in situ* generation of H_2S gas is achieved via a double displacement reaction between sodium sulfide and hydrochloric acid, with inert nitrogen (N_2) as the carrier gas flowing at 5 sccm (Figure 2A-i). Our temporal studies show that the H_2S generation proceeds steadily with time, slowing after 40 min and reaching equilibrium at 60 min (Figure 2B). This corresponds to a H_2S generation efficiency of ~91% with a total of 12 μmol H_2S produced in the first 60 min, thereby translating to a gas flow rate of ~ 0.2 $\mu mol_{H2S}\ min^{-1}$. The H_2S generation process is highly reproducible with <5% fluctuation in H_2S flow rates. Moreover, the second base trap shows no detectable sulfide species, indicating that a single base trap is sufficient to capture all unreacted H_2S in the gas stream (Figure S10). These findings confirm that the H_2S-generation chamber produces gas in a controlled and reproducible manner, ensuring reliable comparisons across sequestration experiments.

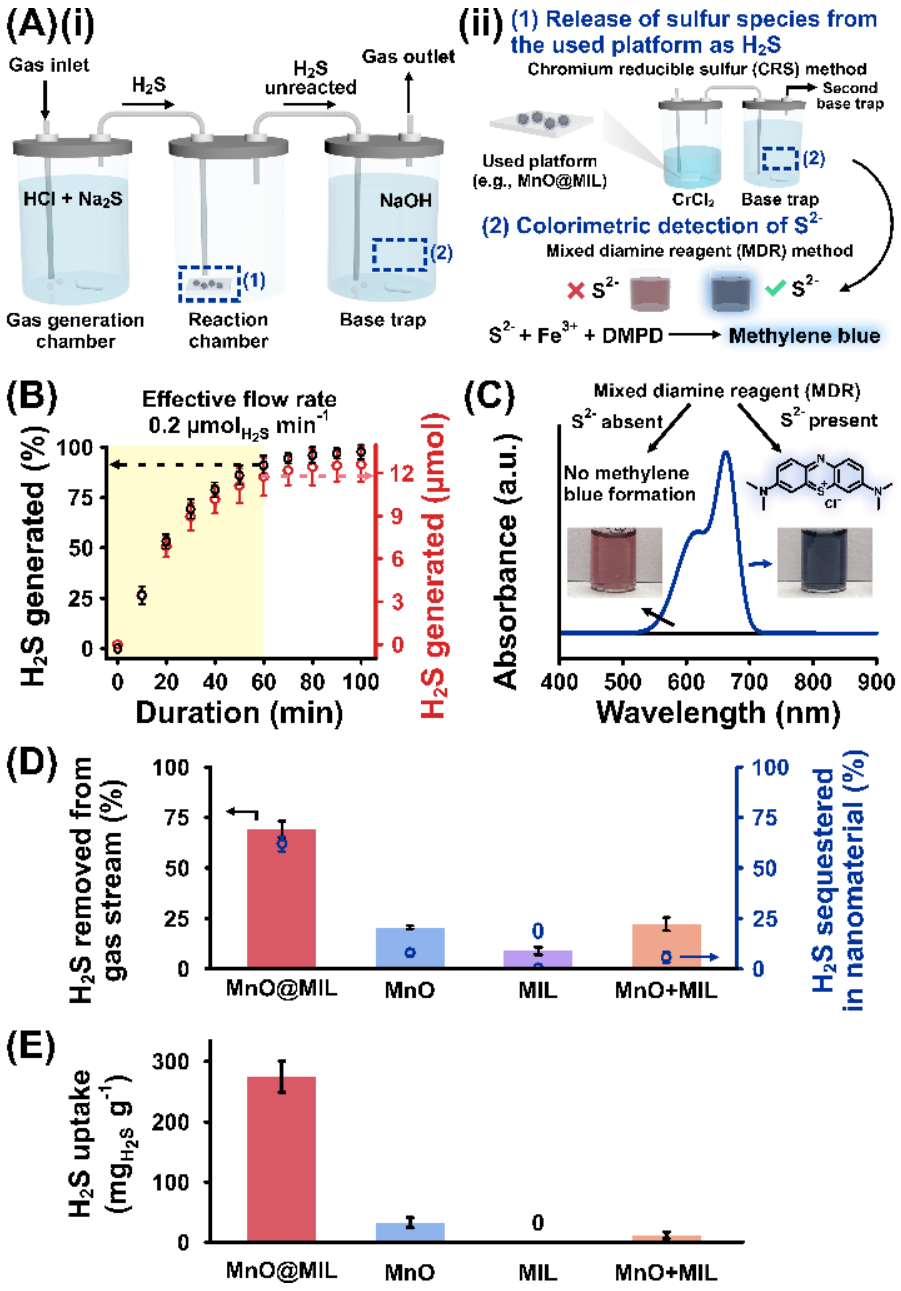


Figure 2. Evaluation of H_2S sequestration performance. (A) Schematic illustration of the (i) experimental setup for direct H_2S sequestration from the gas stream using SAIN and (ii) methods for releasing sequestered sulfur species and quantifying sulfide (S^{2-}) ion concentration (DMPD: N,N-dimethyl-p-phenylenediamine). (B) Time-dependent generation of H_2S by mixing Na_2S and hydrochloric acid (HCl) over 100 min. (C) Photographs and UV-visible absorption spectra showing the presence of S^{2-} via methylene blue formation. (D) Comparison of the amount of H_2S

removed from the gas stream and the actual amount of H_2S sequestered in various nanomaterial platforms, both relative to the original amount of H_2S present in the gas phase. (E) Comparison of H_2S uptake by various nanomaterial platforms.

The SAIN platform (MnO@MIL) is subsequently applied for the reactive entrapment of toxic H_2S gas from a continuous gas stream under ambient conditions (1 atm, 25 ^oC; Figure 2A). A typical experimental setup involves a three-chamber system comprising a H_2S-generation chamber, a reaction chamber containing nanomaterials pre-deposited on a Si substrate, and a final chamber containing an aqueous base trap to capture any unreacted H_2S. The H_2S gas is directed over the nanomaterial platforms, and the reaction is allowed to proceed for 60 min (Figure 2A-i). H_2S sequestration is monitored through two approaches: (1) quantifying the sulfide (S^{2-}) species captured in the base trap, and (2) determining the actual sulfur content sequestered within the nanomaterials. To release the tightly bound sulfide species from the solid matrix, we employ the chromium reducible sulfur (CRS) method involving the heating of nanomaterial platform with zinc powder and hydrochloric acid (6 M). This process releases the sequestered sulfide (S^{2-}) species as H_2S, which is immediately captured in the sodium hydroxide solution (i.e. first base trap) for further analysis (Figure 2A-ii). To ensure accurate comparisons, the release of H_2S from various solid matrix is conducted over an extended period until no significant sulfide is detected (Figure S11, S12). The soluble sulfide species in the sodium hydroxide solution (from both the base traps and CRS method) are quantified using the mixed diamine reagent (MDR) method, where MDR selectively reacts with sulfide species to form methylene blue and undergoes a violet-to-blue transition (Figure 2C). The characteristic absorbance peak of methylene blue at 663 nm is measured via UV-visible absorption

spectroscopy, and the sulfide concentration is calculated using a pre-established calibration curve (Figure S13, S14). Herein, we refer to "sequester" as the amount of H_2S captured within the nanomaterial platforms, while "remove" denotes the total H_2S removed from the gas stream after passing through the reaction chamber.

We first evaluate the performance of the SAIN platform by optimizing two key parameters, namely MnO@MIL mass loading and overall platform area/dimensions, to enhance the H_2S sequestration process. The sequestration/removal efficiency is calculated by comparing the moles of S^{2-} ions detected against the actual moles of H_2S generated over 60 min. A bare Si substrate exhibits negligible H_2S removal (<2%; Figure S10B), confirming that the supporting platform alone does not contribute to H_2S capture. Notably, even a low MnO@MIL mass loading of 0.5 mg achieves significant H_2S removal at ~28% efficiency (Figure S15A). As the MnO@MIL mass loading increases from 0.5 to 2.0 mg, H_2S removal efficiency rises and eventually plateaus at ~80% efficiency beyond 2 mg. Normalizing H_2S removal by mass loading reveals that 1 mg of MnO@MIL delivers the highest mass-specific H_2S removal efficiency (8.5 mmol g^{-1}; dimension, 1 x 1 cm^2) under our experimental conditions (Figure S15B). However, further increasing the mass loadings results in a decrease in mass-normalized H_2S removal efficiency, likely due to limited interaction between H_2S molecules with excess MnO@MIL which imposes an uptake limit. Additionally, we note that platform dimensions have minimal impact on H_2S removal efficiency (Figure S16), with only a <10% deviation (a difference of <1 μmol H_2S) observed when increasing the platform size from (1 × 1) cm^2 to (2 × 2) cm^2 with both using 1 mg loading of MnO@MIL. These results show the H_2S gas readily accesses the nanomaterials, likely facilitated by the nanoporous MIL coating which promotes efficient gas transfer between MnO@MIL particles.

More importantly, the application of the CRS method to determine the actual sulfur content sequestered in the SAIN platform confirms that the H_2S molecules removed from the gas stream are indeed captured within the solid matrix. For instance, we observe a H_2S sequestration efficiency of ~62%, accounting for up to 90% of the H_2S molecules removed from the gas stream (69%; Figure 2D, Figure S11). In addition, the mass difference of SAIN before and after reaction shows up to 95% correlation to the H_2S molecules removed from the gas stream, directly highlighting the measured mass increase in spent SAIN corresponds primarily to the actual H_2S sequestration (Supporting information 1). This observation concretely validates the effectiveness of the CRS method in accurately quantifying the sulfur content sequestered within MnO@MIL. In contrast, a control experiment with MnO@MIL under N_2 flow (i.e., without H_2S) shows no detectable sulfide, confirming that the colorimetric detection response arises solely from the sequestered sulfide while ruling out the possibility of sulfur contamination or side reactions that could lead to false-positive results (Figure S17). It is also noteworthy that the unreacted H_2S is primarily captured in the base trap, as demonstrated by the sum of H_2S removed and sequestered aligning with the total H_2S generated (up to 95%; Figure S18). This observation ensures the integrity of the gas flow setup, eliminating leakage or side reactions that could convert H_2S into other sulfur species instead of being sequestered in the solid matrix. These findings underscore the SAIN platform's high efficiency in sequestering H_2S directly from a continuous gas stream, even under ambient conditions.

Further comparison of the MnO@MIL with various control nanomaterials under identical reaction conditions (i.e., 1 mg loading, platform area of 1 cm^2, and ambient conditions) highlights that the enhanced H_2S sequestration in SAIN is driven by the formation of its functional interface (Figure 2D). These control platforms include pristine MnO nanoparticles,

pristine MIL nanoparticles, and a physical mixture of both MnO and MIL nanoparticles (MnO+MIL, ratio 1:1). MnO@MIL ensemble exhibits the highest sequestration performance (62%), demonstrating a ~8-fold enhancement in H_2S sequestration when compared to pristine MnO (8%). Pristine MIL nanoparticles show negligible adsorption (0%) and remain chemically inactive with H_2S under ambient conditions, underscoring that the metal oxide is the primary active component responsible for the reaction. Interestingly, the MnO@MIL design also demonstrate higher efficiency than the MnO+MIL physical mixture (6%, similar to those of neat MnO platform) by ~10-fold. This finding provides concrete evidence that effective chemical hybridization between the two materials is crucial for creating a functional MnO@MIL interface that activates the metal oxide surface for enhanced reactivity. Moreover, the time-dependent studies on MnO@MIL reveals the H_2S sequestration follows the Langmuir adsorption kinetics model, consistent with surface-controlled reactions at the MnO@MIL interface (Figure S19). Unlike standalone materials, this interfacial activation uniquely boosts H_2S sequestration efficiency (Figure 2E, Figure S18), addressing the limitations of traditional metal oxide and MOF platforms at room temperature and pressure. The SAIN platform consequently achieves the highest H_2S uptake of 274 mg_{H2S} g^{-1}, representing >8-fold, and 23-fold improvements over standalone MnO, MIL (0%), and the MnO+MIL mixture, respectively. We also observe an apparent deviation between H_2S sequestration efficiency and H_2S removal efficiency for MnO, MIL, and MnO+MIL mixtures. This deviation is likely attributed to the formation of highly oxidized sulfur species, such as $MnSO_x$ (to be discussed in next paragraph), which may hinder the CRS method's ability to fully release sulfur content from these control platforms. Besides the high H_2S sequestration performance when using N_2 as a carrier gas, a control experiment with MnO@MIL under air flow demonstrates similar efficient H_2S removal (7.2 μmol), acheiving

~90% sequestration performance relative to the value measured under inert N_2 conditions (Figure S20). This finding evidently highlights the presence of O_2 and other components (*e.g.,* CO_2, CO, SO_2) in the air have negligible effect on MnO@MIL during H_2S sequestration, thereby confirming the robust performance of MnO@MIL in more complex gas matrices.

Experimental and simulation investigations on the interactions between nanomaterials and H_2S

Having established SAIN's higher H_2S sequestration performance, we use XPS, XRD and Raman characterizations to confirm the chemical products formed and examine changes to the interfacial chemistry on MnO@MIL after H_2S exposure. XRD analysis reveals new diffraction peaks corresponding to MnS (PDF #04-028-0435) and no Al_2S_3 signals (PDF #04-007-4630) after H_2S sequestration, while the original diffraction patterns of MnO@MIL remain unchanged (Figure S21). This implies that the reaction primarily occurs at the interfacial region, preserving the core structure of MnO@MIL. In the S 2p XPS spectra, both MnO and MnO@MIL exhibit characteristic S^{2-} features (162.3 eV and 163.3 eV) and SO_x peaks (167.4 eV and 168.8 eV) after H_2S sequestration, while the absence of sulfur signal from MIL is aligned with its negligible sequestration efficiency and limited chemical interaction with H_2S (Figure 3A, Figure S22, S23). Moreover, the S 2p signal positioned between the Mn-S and Mn-SO_x peaks could potentially originate from the higher-order polysulfides species (S_n^{2-}), highlighting our MnO@MIL is capable of efficiently converting and storing sulfur species more than the conventional Mn-S 1:1 stoichiometric ratio. Nevertheless, MnS is the primary product in comparison to the polysulfide, as supported by the XRD signal. Raman bands arises at 220 cm^{-1}, 473 cm^{-1} and 580 cm^{-1} corresponding to the characteristic S-S stretching, S-S-S bending from polysulfides and 2M magnon scattering of MnS, respectively, validating the formation of higher-order polysulfides

species (S_n^{2-}) in MnO@MIL after H_2S sequestration (Figure S24). Notably, MnO displays a much higher SO_x-to-S^{2-} ratio compared to MnO@MIL, indicating greater oxidation of sulfide species in standalone MnO. The presence of S^{2-} and SO_x^{2-} species confirms that H_2S chemically reacts with MnO@MIL, forming MnS as the main product in the SAIN platform. Conversely, $MnSO_x$ is the predominant product in uncoated MnO nanoparticles. This difference likely arises from the increased exposure of MnS in uncoated MnO to atmospheric oxygen, leading to further oxidation. The MnO@MIL design thus plays a vital role in minimizing the formation of $MnSO_x$ (sulfite/sulfate) species, either as a side reaction or through oxidation of MnS intermediates. Minimizing the formation of $MnSO_x$ is essential to prevent re-emission of sulfur species into environment, as sulfates are $>10^5$-fold more soluble in water than sulfide ($MnSO_4$: 762 g L^{-1} at 20 ^oC vs. MnS: 0.006 g L^{-1} at 20 ^oC).

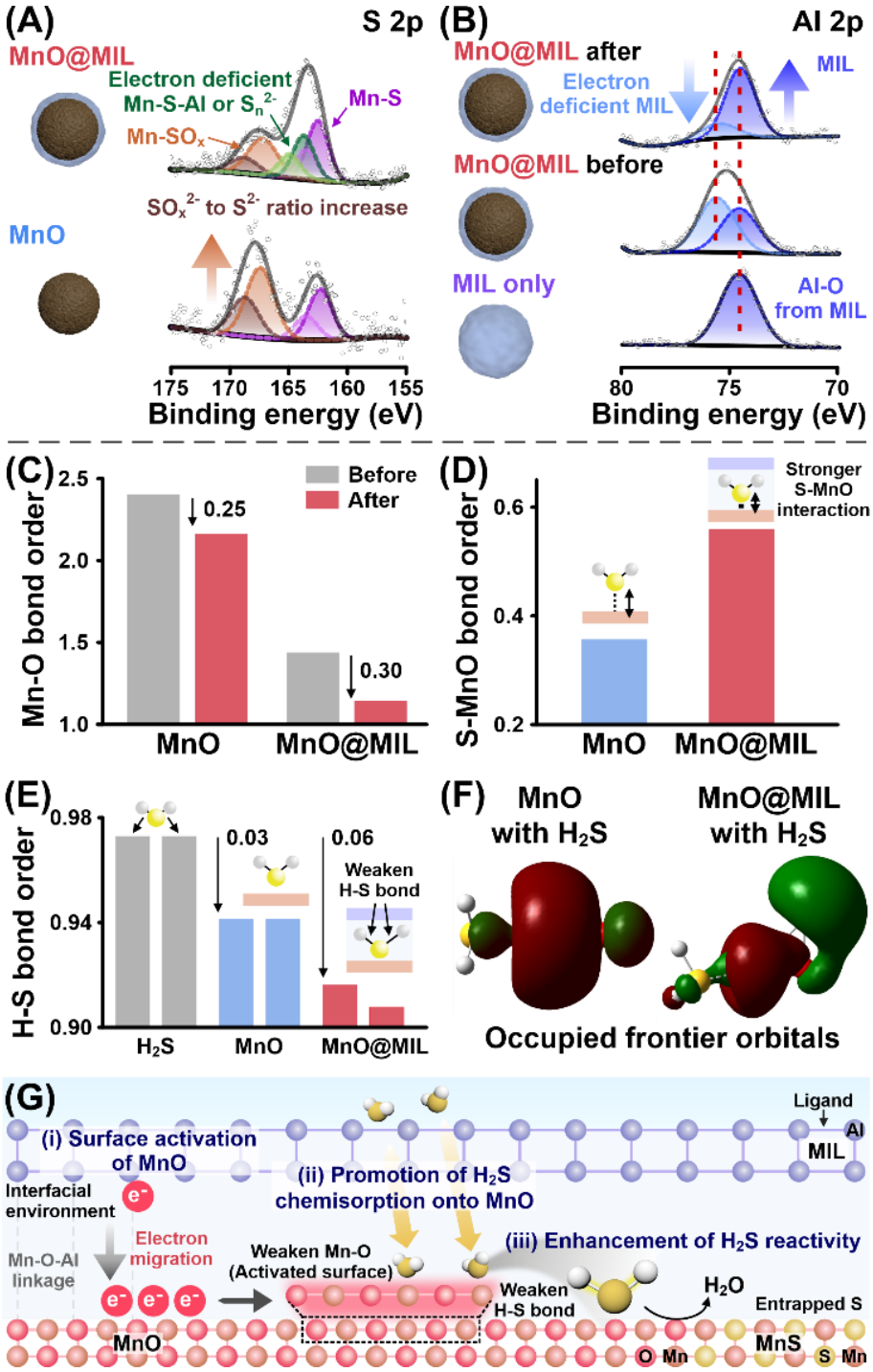


Figure 3. Experimental and simulation investigations on the interactions between platform and H_2S. (A) High-resolution S 2p XPS spectra comparing MnO and MnO@MIL after the H_2S sequestration process. (B) High-resolution Al 2p XPS spectra of the MnO@MIL before and after H_2S sequestration, with MIL included for comparison. (C) DFT-simulated Mn-O bond order of

MnO and MnO@MIL before and after interaction with the H_2S reactant. (D) DFT-simulated S-MnO and (E) H-SH intramolecular bond orders in MnO and MnO@MIL when interacting with H_2S. (F) Occupied frontier orbitals of MnO and MnO@MIL upon interaction with H_2S. (G) Scheme illustrating the mechanism for enhancing H_2S sequestration in SAIN through interfacial electronic hybridization and its chemical effects.

Notably, the sequestration of H_2S in the SAIN platform induces distinct changes in the chemical microenvironment at the MnO@MIL interface, as evidenced by shifts in the XPS spectra of the Al 2p, S 2p, and O 1s orbitals (Figure 3B, Figure S25). For instance, the emergence of Mn-S-Al feature in the S 2p XPS spectrum, positioned between the Mn-S and Mn-SO_x peaks, denotes an oxygen-to-sulfur exchange during H_2S sequestration. This change in chemical linkage between the two materials is further reflected by a concurrent decrease in the intensity of Al 2p (75.6 eV) and O 1s (532.6 eV) peaks that are associated with the electron-deficient MIL component. Additionally, the complementary changes observed in the O 1s XPS spectrum support the transformation in the chemical linkage, as the originally electron-rich MnO species becomes diminished upon H_2S reaction. The notable reversal in the electron-rich nature of MnO and the electron-deficient state of MIL highlights that electron density no longer migrates from the MIL to MnO after the formation of the Mn-S-Al bond. This phenomenon is attributed to the lower electronegativity of sulfur (i.e. more electron donating) compared to oxygen atoms, thereby suppressing the electron-withdrawing effect and stabilizing the new interfacial chemical environment. Our systematic investigation of the MnO@MIL interface before and after H_2S exposure clearly reveals that the oxygen atoms linked to MIL become activated, facilitating the formation of insoluble MnS as the predominant product.

To study the molecular origins of SAIN's enhanced H_2S sequestration, we perform density functional theory (DFT) simulations to investigate the interfacial electronic and chemical effects that occur upon MnO@MIL hybridization and its subsequent interactions with H_2S molecules. These simulations focus on three key factors: (1) Mn-O bond order, (2) interactions between H_2S and MnO species, and (3) the intramolecular H-S bond order and adsorption energy of H_2S. These parameters are critical for understanding the reactivity of MnO, the H_2S-MnO binding strength, and the activation of H_2S molecule, respectively. Our DFT study unravels three important insights into the surface activation of MnO and the enhanced H_2S sequestration facilitated by MnO@MIL. (1) We observe that hybridizing MnO with MIL reduces the Mn-O bond order from ~2.4 in pristine MnO to ~1.4 in MnO@MIL. This reduction in bond order likely occurs due to electron migration from MIL into the lowest unoccupied molecular orbital (LUMO) of MnO, weakening the Mn-O bond and activating the metal oxide surface for subsequent reactions (Figure 3C, Figure S26). (2) MnO@MIL exhibits a 1.6-fold higher H_2S-MnO bond order compared to pristine MnO, indicating stronger interactions with H_2S in the SAIN platform (Figure 3D). The enhanced interaction arises from the stabilization of the positive dipole on Mn species by the nucleophilic H_2S. Our calculations reveal a greater reduction of positive Mulliken charge (~0.10) in MnO@MIL compared to MnO (~0.06), highlighting the stronger stabilization effect by H_2S in the hybrid material (Figure S27). (3) The interactions between H_2S and both MnO and MnO@MIL lead to a weakening of the intramolecular H-S bond. We also explore three different adsorption configurations on both MnO and MnO@MIL, including (i) S head-on, (ii) H tail-on, and (iii) S side-on. This S-H bond weakening effect is more pronounced in S head-on configuration with MnO@MIL ($\Delta_{\text{S-H bond order}}$ = ~0.06) than in S side-on configuration with MnO ($\Delta_{\text{S-H bond order}}$ = ~0.03), denoting stronger activation of the H_2S

molecule (Figure 3E, Figure S28). Moreover, all three configurations on MnO@MIL exhibit negative adsorption energies, indicating thermodynamically favorable adsorption of H_2S on MnO@MIL. The S head-on configuration has the largest adsorption energy of -134 kJ mol^{-1}, indicating it is the most likely adsorption configuration in MnO@MIL. In contrast, we observe only S side-on configuration is favorable for MnO (adsorption energy = -192 kJ mol^{-1}) and the other two configurations have minimal (~0) or even non-favorable adsorption.

Interestingly, in the most stable configuration of MnO@MIL, one of the H-S bonds in H_2S becomes more activated than the other, a phenomenon not observed with pristine MnO (both H-S bond orders are similar). This differential activation can be explained by the distinct frontier orbital interactions. In pristine MnO, H_2S interacts solely through the sulfur atom's lone pair of electrons. However, when interacting with MnO@MIL, H_2S engages both its lone pair of electrons and electron density from the H-S σ bonding orbital (Figure 3F, Figure S29). This additional interaction in MnO@MIL reduces the electron density in the H-S σ bonding orbital, leading to reduced bond order and greater activation of one H-S bond. Moreover, it is noteworthy that although a favorable H_2S adsorption is important, the ability to access the bonding frontier orbital of the H_2S is could be more important to better activate the reactant. The distinct difference in frontier orbital mixing between H_2S and MnO versus MnO@MIL is likely due to the much lower LUMO energy observed in MnO@MIL, thereby allowing for more thermodynamically favorable and effective interaction with the H-S σ bonding orbital (Figure S28).

Elucidating interfacial effects on nanomaterial's surface activation and enhanced performance

The combined insights from experimental and computation studies provide a comprehensive, molecular-level understanding of the interfacial chemical and electronic effects driving the direct solid-gas reaction between H_2S gas and SAIN (Figure 3G). MnO@MIL interface enhances H_2S sequestration through three key processes, namely (i) the surface activation of MnO, (ii) the promotion of H_2S chemisorption onto MnO species, and (iii) the enhancement of H_2S reactivity. The formation of the Mn-O-Al linkage within MnO@MIL plays a crucial role in driving electron density migration from the MIL into the vacant anti-bonding molecular orbital of MnO. This process weakens the Mn-O bond, activating the metal oxide surface and enabling reactions to occur efficiently at the MnO@MIL interface under ambient conditions. The nanoporous MIL coating further enhances the process by capturing H_2S molecules from the gas phase and directing them to the MnO species at the functional interface. At this interface, the electron-rich H_2S interacts strongly with the MnO surface, driven by the stabilization effect on the positive dipole of electron-deficient Mn species. Achieving strong chemisorption of H_2S on MnO is critical for initiating the chemical conversions for effective H_2S sequestration. Additionally, the intimate interaction between H_2S and MnO weakens the intramolecular H-S bond in H_2S by withdrawing electron density from the H-S bonding molecular orbital, facilitating the reactive entrapment of H_2S. The simultaneous activation of both Mn-O and H-S bonds kinetically boosts the interfacial reaction between MnO@MIL and H_2S, leading to the formation of insoluble MnS and the release of H_2O as an environmentally benign byproduct.

Effective H_2S sequestration under various concentration without leaching

Our SAIN design thus introduces an unprecedented “activate-react-lock” strategy that efficiently sequesters toxic H_2S by drastically enhancing the direct gas-solid reaction process.

Notably, our platform achieves a maximum cumulative H_2S uptake of ~1524 mg_{H2S} g^{-1} over sixteen hours of sequestration processes (*i.e.,* 16 consecutive cycles; 45 μmol; Figure 4A). In this experiment, the SAIN platform is placed under the H_2S flow for 1 hour and transferred into another flow setup for the next cycle as the H_2S source needs to be replenished every hour. Note that there is no regeneration step for SAIN between the cycle, which aims to measure the cumulative H_2S sequestration capacity of SAIN. Our findings show that the H_2S uptake increases linearly for the first 10 hours, starts to decrease after the 11^{th} hour, and eventually plateau beyond 14 hours. This observation is due to SAIN initially providing abundant reactive sites, but as sequestration progresses, the number of available sites decreases until saturation causes a plateau. Theoretical estimation on maximum saturation H_2S uptake suggests that a mixture of sulfide and polysulfide species are formed in SAIN throughout the prolonged sequestration over 16 hours (Supporting information 2). Moreover, the MnO@MIL proves highly effective across a broad range of initial H_2S concentrations, efficiently capturing ~62% of H_2S at 1000 ppm, ~70% of H_2S at 50 ppm, ~86% sequestration at 10 ppm, and reaching near 100% sequestration even at trace levels of 5 ppm under ambient conditions (Figure 4B). This concentration-dependent study underscores the platform's versatility, making it suitable for addressing both anthropogenic industrial emissions (up to 1000 ppm) and natural geothermal releases (up to 70 ppm). The results also suggest that optimizing gas flow path lengths could further improve H_2S interaction time, maximizing sequestration efficiency in practical scenarios with variable or unknown H_2S concentrations. Realizing effective H_2S sequestration is crucial for eliminating harmful gases, especially beyond the 100 ppm olfactory fatigue threshold, where exposure becomes life-threatening. It also mitigates long-term exposure to lower H_2S concentrations (≤10 ppm) which can lead to chronic health issues.

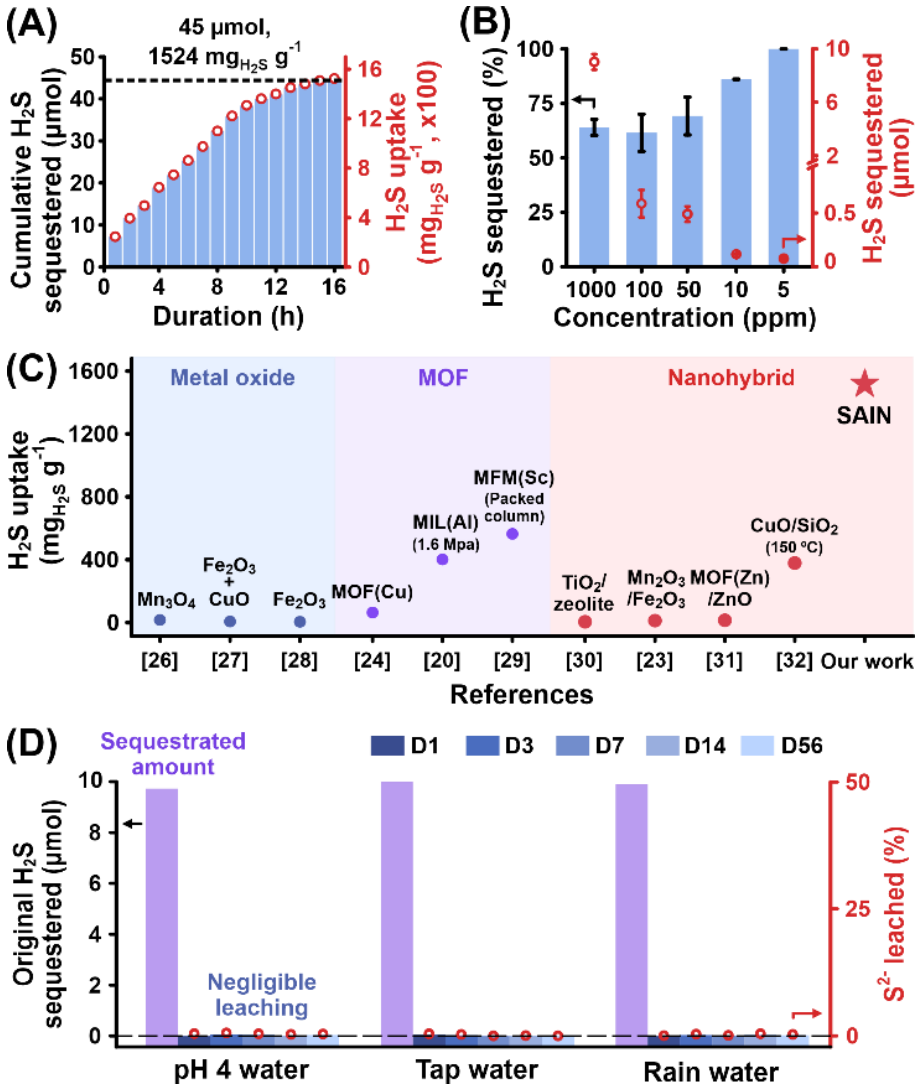


Figure 4. Evaluation of SAIN sequestration performance under various concentration and its stability in water. (A) Cumulative H_2S uptake over sixteen cycles using SAIN (MnO@MIL) under 1000 ppm H_2S flow. (B) Amount of H_2S sequestrated under varying H_2S gas flow concentrations. (C) Comparison of H_2S uptake by SAIN with previously reported platforms, including transition metal oxides, MOFs, and their nanohybrids. (D) Leaching test showing the original H_2S sequestered in SAIN and the negligible S^{2-} leaching from MnO@MIL when immersed in various water environments (pH 4 water, tap water, and rainwater) over 56 days.

More importantly, the MnO@MIL design achieves up to 508-fold higher maximal H_2S uptake and a 24-fold faster sequestration rate compared to other emerging systems based on transition metal oxides, MOFs, and hybrid materials, even when these conventional platforms employed elevated temperatures and pressures (Figure 4C, Table S1).[20, 23, 24, 26-32] Notably, our spent SAIN maintains its physical and chemical integrities while the MIL layer remains intact on the MnO core after H_2S sequestration (Figure S30). Moreover, the oxygen-to-sulfur exchange process in SAIN induces a structural transformation in the metal oxide surface, allowing it to securely trap harmful sulfur species within its solid matrix even in diverse water environment like simulated acid rain (pH 4), tap water, and rainwater (Figure 4D). It is noteworthy that no sulfur species leach out from the spent MnO@MIL platform (<0.6% of H_2S; <0.06 μmol of H_2S) in these untreated artificial and real water samples over a prolonged 56-day period. Moreover, the absence of terephthalic acid (organic linker) signal in ^1H NMR spectra further demonstrate the high stability of the MIL component on the MnO@MIL in various water environments over 280-day period (Figure S31). SAIN also demonstrates excellent stability under various practical environmental conditions, including (i) aqueous environments at elevated temperatures (*e.g.,* 50 °C, 100 °C) and (ii) exposure to real air flow. No sulfur species is detected in the water after 4 hours of heating, indicating good thermal stability under high-temperature aqueous conditions (Figure S32A). Additionally, after 1 hour of continuous air flow, the sulfur species remain securely confined within the SAIN and do not leach from the solid. These results clearly highlight the robust chemical stability of SAIN in the presence of water vapor (relative humidity = 46%) and typical atmospheric gases, including CO_2, O_2, and N_2 (Figure S32B). Collectively, these findings underscore the high chemical and thermal stability of the SAIN platform, ensuring

effective sequestration of hazardous sulfur species and supporting its practical feasibility for real-world environmental applications.

Conclusion

In conclusion, our SAIN demonstrates highly efficient H_2S sequestration at ambient conditions by harnessing the synergy between nanomaterial surfaces and reticular chemistry. The SAIN platform enhances solid-gas reactions through two key concepts: (1) leveraging a MOF layer to capture H_2S from the gas phase and transfer it to the functional interface, and (2) exploiting interfacial electronic and chemical hybridization to activate the MnO surface, boosting its reactivity with H_2S and promoting the formation of insoluble MnS. This unprecedented "activate-react-lock" strategy enables efficient and rapid H_2S sequestration across a wide concentration range (5 – 1000 ppm), achieving an uptake of up to 1524 mg_{H2S} g^{-1} and nearly 100% sequestration efficiency at concentrations as low as 5 ppm (below the recommended exposure limit of 10 ppm). The SAIN platform exhibits 23-fold higher sequestration efficiency compared to standalone metal oxide or MOF nanomaterials, highlighting the unique reactivity at the MnO@MOF interface. It also demonstrate higher performance over other emerging designs by up to 508-fold in maximal H_2S uptake and 24-fold in sequestration rate. Experimental and simulation studies reveal that this enhanced solid-gas interaction results from electron migration and electronic hybridization at the interface, which (i) weakens the Mn-O bond to activate the MnO surface, (ii) promotes MnO interaction with H_2S, and (iii) disrupts the intramolecular S-H bond in H_2S to facilitate efficient oxygen-to-sulfur exchange. The spent SAIN is chemically robust, securely trapping harmful sulfur species within its solid matrix even in artificial and real water environments, as well as various environmental conditions. This advantage prevents toxic

solid waste formation and secondary pollution from leaching, thereby making this platform highly attractive for practical applications. Moreover, the sulfur species trapped in MnO@MIL can potentially be recovered through chemical treatments (*e.g.*, CRS method), contributing to a circular sulfur economy.

In future work, advanced spectroscopic and analytical techniques such as XAFS could be utilize to reveal the local coordination environment of Mn, thereby providing deeper insights into the fine structure at the interface and the mechanistic pathways governing H_2S sequestration within the SAIN platform. Future studies can also focus on industrial adoption by translating this proof-of-concept demonstration into pilot-scale applications, taking into account scalability and large-scale feasibility. For instance, the synthesis could be scaled up using automation or fluidic approaches while the SAIN platform may be employed in packed-bed reactors for practical implementation. Beyond scalable synthesis and reaction routes, other key factors such as rational process design, material cost, and regeneration feasibility should be also systematically evaluated to ensure large-scale reproducibility, cost-effectiveness, and industrial viability. From an application-oriented perspective, the excellent water and thermal stability of SAIN render it a promising candidate for industrial waste gas treatment and environmental remediation. In addition, further exploration of other Al-based MOFs, as well as broader MOF systems, could be important for elucidating additional fundamental insights to better optimize the SAIN platform for improving solid-gas reactions. By enhancing the intrinsic reactivity of nanomaterials, this work addresses the limitations of conventional materials for H_2S sequestration and provides an effective solution for environmental remediation under ambient conditions. These valuable insights provide a framework for designing functional interfaces that activate nanomaterial surfaces directly at the point-of-reaction, opening new avenues for efficient gas-solid reactions

across diverse applications, including air pollution control, solid-phase synthesis, catalysis, and energy conversion.

Experimental Methods

Chemicals

Aluminum nitrate nonahydrate (≥ 98.0%, ACS reagent), benzyl ether (98.0%), chromium(III) chloride hexahydrate (purum p.a. ≥ 98.0%), iron(III) chloride hexahydrate (≥ 97.0%, ACS reagent), N,N-dimethyl-p-phenylenediamine (≥ 97.0%), oleic acid (technical grade, 90%), sodium sulfide nonahydrate (≥ 98.0%, ACS reagent) and terephthalic acid (98%) were purchased from Sigma Aldrich. Zinc powder was obtained from Sinopharm Chemical Reagent Co., Ltd. Sodium hydroxide was from VWR chemicals. Manganese (II) 2,4-pentanedionate was purchased from Alfa Aesar. Hydrochloric acid (37%, AR grade) was obtained from Schedelco. Ethanol (≥ 99.8%, absolute), acetone (≥ 99.8%), and hexane (HPLC grade) were from Thermo Fisher Scientific. Nitrogen (N_2; ALPHAGAZ 1; 99.999%) was purchased from Leeden National Oxygen Ltd. Air gas tank (O_2: 20.4% – 21.4%, impurities: H_2O, CO_2, CO, SO_2) was purchased from Air Liquide. All chemicals were applied without further purification. Milli-Q water (> 18.0 MΩ.cm) was purified with a Sartorius Arium 611 ® UV ultrapure water system.

Synthesis of manganese(II) oxide (MnO) nanospheres

MnO nanospheres were synthesized based on a procedure from the literature with slight modifications.[33] Initially, 20 mL of benzyl ether, 2 mL of oleic acid, and 0.5063 g of manganese(II) 2,4-pentanedionate were added to a three-necked round bottom flask. The

resulting mixture was heated to 70 ºC with rapid stirring under nitrogen atmosphere. The reaction setup was then evacuated under vacuum and purged with nitrogen gas for three cycles to remove any residual gases. The mixture was further heated to 285 °C and refluxed for 2 hours under a nitrogen atmosphere. After the reaction was completed and the system was cooled to room temperature, the synthesized nanospheres were precipitated by adding ethanol in excess. The resulting product was thoroughly washed with hexane, ethanol, and acetone. Finally, the purified nanospheres were redispersed in ethanol for further use.

Synthesis of MIL nanoparticles

The synthesis of MIL nanoparticles at room temperature in water was adapted from a previously reported method.[34] First, an aqueous solution of disodium terephthalate (694 mM) was prepared by dissolving 1 g of sodium hydroxide and 2 g of terephthalic acid in 17 mL of water. The resulting solution was then diluted 10-fold prior to use. Next, 0.58 mL of the diluted disodium terephthalate solution (69.4 mM) was added dropwise to 0.58 mL of aluminum nitrate nonahydrate (0.14 M) under continuous stirring at 200 rpm for 4 hours. The resulting product was washed with copious amounts of water and then redispersed in water for further use.

Synthesis of MnO@MIL

Prior to synthesis, 2.6 mL of ethanolic solution containing MnO nanospheres (0.22 g/mL) was centrifuged and the nanoparticles were redispersed in water. To this suspension, 0.19 mL of aluminum nitrate nonahydrate (0.14 M) and 0.19 mL of disodium terephthalate (69.4 mM) were sequentially added, followed by stirring at 200 rpm for 4 hours. The resulting product was washed with water via centrifugation and redispersed in water for further use.

Gas flow reaction setup for H_2S sequestration

Various synthesized nanomaterials, including MnO@MIL, MnO, MIL, and a physical mixture of MnO and MIL nanoparticles, were deposited onto a 1 cm^2 silicon wafer. The deposition process was performed under controlled conditions to ensure uniform coverage. After deposition, the wafer was placed in a desiccator and allowed to dry before subsequent testing.

A gas flow reaction setup was constructed using a three-vial system. The first vial functioned as the H_2S gas-generating chamber, the second vial housed the gas-capturing nanomaterial platforms as the reaction chamber, and the third vial contained a 20 mL solution of sodium hydroxide (0.015 M) that served as a base trap to capture any remaining H_2S in the gas stream. Before starting the experiment, N_2 gas was passed through the system for at least 10 minutes to ensure an inert atmosphere and to act as the carrier gas for H_2S vapor. In the gas-generating chamber, 25 mL of sodium sulfide (0.5 mM) was mixed with 0.5 mL of hydrochloric acid (0.1 M) and stirred at 200 rpm to generate H_2S. The gas was then carried through the system with N_2 as carrier gas at a flow rate of 5 sccm, regulated by a mass flow controller (MC-100SCCM-D, Alicat Scientific Inc.). After 60 minutes, the nanomaterial platforms were removed for sulfur species quantification using the chromium reducible sulfur (CRS) analysis, which converts sulfur species into soluble forms for quantification. The solutions from both the gas-generating chamber and the base trap were also reacted with mixed diamine reagent (MDR) solution and analyzed by UV-visible absorption spectroscopy, using MB's characteristic peak at 663 nm to determine sulfur concentrations. The removal efficiency (%) was calculated by comparing the moles of S^{2-} ions detected against the actual moles of H_2S generated.

To determine the maximum H_2S capacity of SAIN, the MnO@MIL platform was first placed in the reaction chamber for 60 minutes (1 cycle) and immediately transferred into another gas flow

reaction setup for the next cycle of H_2S sequestration. The moles of S^{2-} ions were quantified with the aforementioned procedure.

Time-dependent study of H_2S generation

For the time-dependent study of H_2S generation, the three-vial gas flow setup was modified by replacing the second vial (reaction chamber) with 20 mL of sodium hydroxide (0.015 M) to directly capture the generated H_2S (first base trap). The third vial (second base trap) contained 5 mL of sodium hydroxide (0.015 M) instead of the typical 20 mL solution. At 10-minute intervals, 1 mL of solution was withdrawn from the base trap and reacted with MDR solution to monitor the amount of H_2S being generated over time.

Detection and quantification of sulfide species (S^{2-}) using mixed diamine reagent (MDR)

We employed the mixed diamine reagent (MDR) method for the quantification of sulfide species. The preparation of MDR followed the procedure outlined in previous literature.[35] Briefly, 4.8 g of iron(III) chloride hexahydrate and 3.2 g of N,N-dimethyl-p-phenylenediamine were dissolved in 200 mL of hydrochloric acid (6 M). The prepared MDR solution was stored at 4 °C in the dark until further use.

A calibration curve correlating the absorbance intensity of the methylene blue (MB) product signal with the concentration of S^{2-} was subsequently established to enable the quantification of H_2S in the gas flow reaction. Sodium sulfide was first dissolved in water and diluted to a range of concentrations between 2.5×10^{-5} M and 2.5×10^{-4} M. 0.2 mL of MDR was then mixed with 2.5 mL of sodium sulfide standard solution, and the mixture was stirred at 200 rpm for 30 minutes for reaction. After the reaction, the resulting solution was diluted 4-fold prior to the UV-visible absorption spectroscopy measurement. The absorption spectra were recorded and MB's

characteristic peak at 663 nm was used to construct the calibration curve. Additionally, the calibration curve of Na_2S in sodium hydroxide was prepared with the same procedure, except the Na_2S was dissolved in sodium hydroxide instead of water.

To quantify the sulfide species after the gas flow reaction, 5 mL of the resulting solution was mixed with 0.4 mL of MDR solution, and the mixture was stirred at 200 rpm for 30 minutes. Following this, the solution was diluted as necessary to bring the absorbance within the range of the previously established calibration curve. UV-visible absorption spectroscopy was then performed, with the characteristic peak of MB at 663 nm being identified and correlated to the calibration curve for sulfide quantification.

Chromium reducible sulfur (CRS) method for releasing and quantifying sulfur species

The chromium reducible sulfur (CRS) method for releasing sulfur-containing species (*e.g.*, inorganic sulfides) was adapted from previous literature with modifications.[36] Chromium(II) chloride solution was freshly prepared prior to the experiment. In brief, 6 g of chromium(III) chloride hexahydrate was dissolved in 15 mL of hydrochloric acid (6 M) in a round-bottom flask under an inert atmosphere with rapid stirring. Next, 3 g of zinc powder was gradually added portion-wise to the solution. The successful formation of chromium(II) chloride was indicated by a color change from dark green to bright blue.

To release the sulfur species trapped in the nanomaterials, the three-vial flow setup was pre-flushed with N_2 gas to remove any interfering gases. 10 mL of freshly prepared chromium(II) chloride was then added to the vial containing the nanomaterial platform and heated at 60 °C under continuous N_2 flow and stirring for 90 minutes. At the gas outlet, 20 mL of aqueous sodium hydroxide solution (0.015 M) was used as a base trap to capture the sulfur species

released in the form of H_2S gas. A second base trap containing aqueous sodium hydroxide solution (0.015 M) was placed downstream of the first trap to ensure complete capture of any residual H_2S. The trapped sulfur species in the base traps were then reacted with MDR solution, followed by UV-visible absorption spectroscopy to quantify the sulfur content. The sequestration efficiency (%) was calculated by comparing the moles of S^{2-} ions detected in the SAIN against the actual moles of H_2S generated.

Leaching study of reacted MnO@MIL platforms

The reacted MnO@MIL platforms were immersed in three different water samples, namely (i) pH 4 water, (ii) tap water, and (iii) rainwater. The pH 4 water was prepared using ultrapure water and hydrochloric acid, while the tap water and rainwater were real samples collected in Singapore. Aliquots of the water samples were taken on days 1, 3, 7, 14, and 56, and analyzed using the CRS method to quantify any sulfur species leached from the platforms.

The leaching percentage (%) of sulfur species was calculated using the following formula:

$$Leaching\ percentage\ (\%) = \frac{Leachedamount(mol)}{Sequestratedamount(mol)} \times 100\%$$

The three water samples with spent MnO@MIL platforms were measured by the proton nuclear magnetic resonance (^{1}H NMR). Aliquots of the water samples were taken on Day 280, dried and redispersed in deuterated DMSO for the subsequent measurement. The aqueous solutions of the organic linker of MIL, terephthalic acid, were used as standard solutions as a benchmark for comparison.

For leaching studies at elevated temperature, the reacted MnO@MIL platforms were immersed in water and heated to an elevated temperature of 50 °C and 100 °C, respectively. Aliquots of the

water samples were taken and analyzed to quantify any sulfur species leached from the platforms.

Density functional theory (DFT) simulations

The interaction between the MnO and MnO@MIL surfaces with hydrogen sulfide was calculated using the unrestricted B3LYP exchange-correlation functional, as implemented in the Gaussian 09 computational chemistry package. The 6-31G (d,p) basis set was used for all atoms, except for Mn, where the LANL2DZ basis set was employed. For the MnO@MIL system, an Al atom was placed near to the Mn-O molecule during geometry optimization, with the angles between atoms fixed to simulate the formation of the MnO@MIL interfacial layer, in accordance with a previously reported approach.[37, 38] The interfacial structure was designed to reflect the assembly of Al^{3+} ions and terephthalate ligands into a crystalline scaffold, as supported by XPS characterization (Figure 1D, Figure S5), which confirmed the presence of electron-donating MIL species. H_2S molecule was subsequently added near the Mn-O surface to study molecular-level interactions between the surfaces and the gas molecule. Bond order analysis was performed using Multiwfn software package based on the Gaussian output files.[39]

Material characterization

Scanning electron microscopy (SEM) and energy-dispersive X-ray spectroscopy (EDS) characterization were conducted using a JEOL JSM-7600F microscope. To enhance conductivity for SEM imaging, an ultrathin Pt layer (<5 nm) was coated on the nanomaterials using JEOL JFC-1600 Auto Fine Coater. Transmission electron microscopy (TEM) images were obtained on a JEM-1400 (JEOL) operating at an accelerating voltage of 100 kV. All N_2 adsorption-desorption isotherms were obtained with using Quantachrome Quadrasorb EVO/SI analyzer

equipped with a FloVac degasser. Samples were outgassed at 200 °C for 20 hours prior transfer to the analyzer. Surface area and pore size were calculated by applying the Brunauer–Emmett–Teller (BET) method. X-ray photoelectron spectroscopy (XPS) was performed on a Phoibos 100 spectrometer using monochromatic Al Kα radiation source (1486.7 eV). The XPS binding energies were referenced to the C 1s peak at 284.5 eV. Ultraviolet photoelectron spectroscopy (UPS) was performed using an AXIS Supra spectrometer equipped with a hemispherical analyzer and a He(I) source (hv = 21.22 eV) with an analysis area of 55 μm and a pass energy of 5 eV. UV-visible absorption spectra were measured with an AvaSpec-ULS2048CL-EVO-UA-50 equipped with a deuterium-halogen light source (AvaLight-DH-S). X-ray diffraction (XRD) patterns were collected using a Rigaku MiniFlex 600C diffractometer with Cu Kα radiation source. ^{1}H NMR spectra were recorded on JEOL ECA400MHz spectrometer. Relative humidity of the flow system was measured with Shaw SDHmini-L Portable Hygrometer. Raman spectra were carried out using uRaman microscope (Technospex PTE LTD) using laser of 532 nm wavelength. Each Raman spectrum is the average of 5 scans with 500 ms acquisition time. Diameter of the synthesized nanomaterials on the SEM images were measured using ImageJ software.

Supporting Information

Supporting Information Available: TEM and SEM images of nanomaterials, XPS and UPS spectra of nanomaterials before and after reaction, N_2 adsorption-desorption isotherms of nanomaterials, scheme of gas flow setup, UV-vis absorption spectra, H_2S quantification of various control experiments, calibration curve of sulfide quantification, amount of H_2S sequestered using MnO@MIL under different loading and platform dimensions, NMR spectra for stability studies, leaching studies at elevated temperature and air flow, XRD and Raman

spectra of MnO@MIL after reaction, computational studies (frontier orbital, electrostatic potential map, energy diagram, adsorption configuration) of various nanomaterials, comparison with literature, correlation of mass change in MnO@MIL before and after reaction, calculation of theoretical maximum H_2S capacity of SAIN

AUTHOR INFORMATION

Corresponding Author

Hiang Kwee Lee − Division of Chemistry and Biological Chemistry, School of Chemistry, Chemical Engineering and Biotechnology, Nanyang Technological University, 21 Nanyang Link, Singapore 637371 (Singapore). Email: hiangkwee@ntu.edu.sg

Author

Li Shiuan Ng − Division of Chemistry and Biological Chemistry, School of Chemistry, Chemical Engineering and Biotechnology, Nanyang Technological University, 21 Nanyang Link, Singapore 637371 (Singapore).

Jun Jing Teh − Division of Chemistry and Biological Chemistry, School of Chemistry, Chemical Engineering and Biotechnology, Nanyang Technological University, 21 Nanyang Link, Singapore 637371 (Singapore).

Zhi Zhong Ang − Division of Chemistry and Biological Chemistry, School of Chemistry, Chemical Engineering and Biotechnology, Nanyang Technological University, 21 Nanyang Link, Singapore 637371 (Singapore).

Veronica Pereira− Division of Chemistry and Biological Chemistry, School of Chemistry, Chemical Engineering and Biotechnology, Nanyang Technological University, 21 Nanyang Link, Singapore 637371 (Singapore).

Sankar Das− Division of Chemistry and Biological Chemistry, School of Chemistry, Chemical Engineering and Biotechnology, Nanyang Technological University, 21 Nanyang Link, Singapore 637371 (Singapore).

Brynne Shu Ni Tan− Division of Chemistry and Biological Chemistry, School of Chemistry, Chemical Engineering and Biotechnology, Nanyang Technological University, 21 Nanyang Link, Singapore 637371 (Singapore).

Author Contributions

The manuscript was written through the contributions of all authors. All authors have given approval to the final version of the manuscript. ‡L.S.N. and J.J.T. contributed equally.

ACKNOWLEDGMENT

H.K.L. thanks the funding supports from Singapore Ministry of Education (AcRF Tier 1 RS13/20 and RG4/21), A*STAR Singapore (AME YIRG A2084c0158 and MTC IRG M23M6c0098), National University of Singapore Center of Hydrogen Innovation (CHI-P2022-05), and Nanyang Technological University start-up grants. The research was conducted as a part of NICES (NTU-IMRE Chemistry Lab for Eco Sustainability; REQ0275931), a joint research initiative between Nanyang Technological University (NTU) and Institute of Materials Research and Engineering (IMRE) from Agency for Science, Technology and Research (A*STAR). We would like to acknowledge the Facility for Analysis, Characterisation, Testing and Simulation, Nanyang Technological University, Singapore, for use of their X-ray facilities.

REFERENCES

(1) Fosnacht, K. G.; Pluth, M. D. Activity-Based Fluorescent Probes for Hydrogen Sulfide and Related Reactive Sulfur Species. *Chem. Rev.* **2024**, *124* (7), 4124-4257.

(2) Belmabkhout, Y.; Bhatt, P. M.; Adil, K.; Pillai, R. S.; Cadiau, A.; Shkurenko, A.; Maurin, G.; Liu, G.; Koros, W. J.; Eddaoudi, M. Natural Gas Upgrading using a Fluorinated MOF with Tuned H_2S and CO_2 Adsorption Selectivity. *Nat. Energy* **2018**, *3* (12), 1059-1066.

(3) Camilleri, S. F.; Montgomery, A.; Visa, M. A.; Schnell, J. L.; Adelman, Z. E.; Janssen, M.; Grubert, E. A.; Anenberg, S. C.; Horton, D. E. Air Quality, Health and Equity Implications of Electrifying Heavy-Duty Vehicles. *Nat. Sustain.* **2023**, *6* (12), 1643-1653.

(4) Yi, S.; Ghanem, B.; Liu, Y.; Pinnau, I.; Koros, W. J. Ultraselective Glassy Polymer Membranes with Unprecedented Performance for Energy-Efficient Sour Gas Separation. *Sci. Adv.* **2019**, *5* (5), eaaw5459.

(5) Aminuddin, M. S.; Bustam, M. A.; Johari, K. Latest Technological Advances And Insights into Capture and Removal of Hydrogen Sulfide: a critical review. *RSC Sustain.* **2024**, *2* (4), 757-803.

(6) *Occupational Safety and Health Administration, Safety and Health Topics/Hydrogen Sulfide*. https://www.osha.gov/hydrogen-sulfide/hazards (accessed 2024-10-04).

(7) Yu, Z.; Deng, Z.; Li, Y.; Wang, X. Advances in Electrocatalyst Design and Mechanism for Sulfide Oxidation Reaction in Hydrogen Sulfide Splitting. *Adv. Funct. Mater.* **2024**, *34* (39), 2403435.

(8) Chen, S.; Guo, Y.; Zhang, J.; Guo, Y.; Liang, X. $CuFe_2O_4$/Activated Carbon Adsorbents Enhance H_2S Adsorption and Catalytic Oxidation from Humidified Air at Room Temperature. *Chem. Eng. J.* **2022**, *431*, 134097.

(9) Zheng, X.; Lei, G.; Wang, S.; Shen, L.; Zhan, Y.; Jiang, L. Advances in Resources Recovery of H_2S: A Review of Desulfurization Processes and Catalysts. *ACS Catal.* **2023**, *13* (17), 11723-11752.

(10) Nunez, Y.; Benavides, J.; Shearston, J. A.; Krieger, E. M.; Daouda, M.; Henneman, L. R. F.; McDuffie, E. E.; Goldsmith, J.; Casey, J. A.; Kioumourtzoglou, M.-A. An Environmental Justice Analysis of Air Pollution Emissions in the United States from 1970 to 2010. *Nat. Commun.* **2024**, *15* (1), 268.

(11) Huang, K.; Wu, Y.-T.; Hu, X.-B. Effect of Alkalinity on Absorption Capacity and Selectivity of SO_2 and H_2S over CO_2: Substituted Benzoate-Based Ionic Liquids As The Study Platform. *Chem. Eng. J.* **2016**, *297*, 265-276.

(12) Kailasa, S. K.; Koduru, J. R.; Vikrant, K.; Tsang, Y. F.; Singhal, R. K.; Hussain, C. M.; Kim, K.-H. Recent Progress on Solution and Materials Chemistry for the Removal of Hydrogen Sulfide from Various Gas Plants. *J. Mol. Liq.* **2020**, *297*, 111886.

(13) Shah, M. S.; Tsapatsis, M.; Siepmann, J. I. Hydrogen Sulfide Capture: From Absorption in Polar Liquids to Oxide, Zeolite, and Metal–Organic Framework Adsorbents and Membranes. *Chem. Rev.* **2017**, *117* (14), 9755-9803.

(14) Pudi, A.; Rezaei, M.; Signorini, V.; Andersson, M. P.; Baschetti, M. G.; Mansouri, S. S. Hydrogen Sulfide Capture and Removal Technologies: A Comprehensive Review of Recent Developments and Emerging Trends. *Sep. Purif. Technol.* **2022**, *298*, 121448.

(15) Wu, X.; Niu, M.; Tian, X.; Peng, X.; Buenconsej, P. J. S.; Wu, X.; Wang, Y.; Ji, W.; Li, Y.; Qiao, J.; et al. Solution-Processable $Ni_3(HITP)_2$/MXene Heterostructures for ppb-Level Gas Detection. *J. Mater. Chem. A* **2024**, *12* (28), 17382-17394.

(16) Liu, X.; Wang, R. Effective Removal of Hydrogen Sulfide Using 4A Molecular Sieve Zeolite Synthesized from Attapulgite. *J. Hazard. Mater.* **2017**, *326*, 157-164.

(17) Jiang, Q.; Li, T.; He, Y.; Wu, Y.; Zhang, J.; Jiang, M. Simultaneous Removal of Hydrogen Sulfide and Ammonia in the Gas Phase: a review. *Environ. Chem. Lett.* **2022**, *20* (2), 1403-1419.

(18) Yuan, H.; Li, K.; Shi, D.; Yang, H.; Yu, X.; Fan, W.; Buenconsejo, P. J. S.; Zhao, D. Large-Area Fabrication of Ultrathin Metal-Organic Framework Membranes. *Adv. Mater.* **2023**, *35* (18), 2211859.

(19) Wu, X.; Tian, X.; Zhang, W.; Peng, X.; Zhou, S.; Buenconsejo, P. J. S.; Li, Y.; Xiao, S.; Tao, J.; Zhang, M.; et al. Solution-Processable MOF-on-MOF System Constructed via Template-Assisted Growth for Ultratrace H2S Detection. *Angew. Chem. Int. Ed.* **2024**, *63* (49), e202410411.

(20) Hamon, L.; Serre, C.; Devic, T.; Loiseau, T.; Millange, F.; Férey, G.; Weireld, G. D. Comparative Study of Hydrogen Sulfide Adsorption in the MIL-53(Al, Cr, Fe), MIL-47(V), MIL-100(Cr), and MIL-101(Cr) Metal−Organic Frameworks at Room Temperature. *J. Am. Chem. Soc.* **2009**, *131* (25), 8775-8777.

(21) Westmoreland, P. R.; Gibson, J. B.; Harrison, D. P. Comparative Kinetics of High-Temperature Reaction between Hydrogen Sulfide and Selected Metal Oxides. *Environ. Sci. Technol.* **1977**, *11* (5), 488-491.

(22) Maroño, M.; Ortiz, I.; Sánchez, J. M.; Alcaraz, L.; Alguacil, F. J.; López, F. A. Effective Removal of Hydrogen Sulfide Using Mn-Based Recovered Oxides from Recycled Batteries. *Chem. Eng. J.* **2021**, *419*, 129669.

(23) Kim, S.; Gupta, N. K.; Bae, J.; Kim, K. S. Fabrication of Coral-Like Mn_2O_3/Fe_2O_3 Nanocomposite for Room Temperature Removal of Hydrogen Sulfide. *J. Environ. Chem. Eng* **2021**, *9* (3), 105216.

(24) Yang, Y.; Liu, X.; Yang, C.; Wang, Y.; Wang, H.; Fan, H. Study on The Essential Features for MOFs to Reversible Adsorption of H_2S at Room Temperature. *Colloids Surf. A: Physicochem. Eng. Asp.* **2023**, *674*, 131914.

(25) Wu, M.; Guo, E.; Li, Q.; Mi, J.; Fan, H. Mesoporous Zn-Fe-Based Binary Metal Oxide Sorbent with Sheet-Shaped Morphology: Synthesis and Application for Highly Efficient Desulfurization of Hot Coal Gas. *Chem. Eng. J.* **2020**, *389*, 123750.

(26) Xue, M.; Chitrakar, R.; Sakane, K.; Ooi, K. Screening of Adsorbents for Removal of H_2S at Room Temperature. *Green Chem.* **2003**, *5* (5), 529-534, 10.1039/B303167P.

(27) Costa, C.; Cornacchia, M.; Pagliero, M.; Fabiano, B.; Vocciante, M.; Reverberi, A. P. Hydrogen Sulfide Adsorption by Iron Oxides and Their Polymer Composites: A Case-Study Application to Biogas Purification. *Materials* **2020**, *13* (21).

(28) Cristiano, D. M.; de A. Mohedano, R.; Nadaleti, W. C.; de Castilhos Junior, A. B.; Lourenço, V. A.; Gonçalves, D. F. H.; Filho, P. B. H_2S Adsorption on Nanostructured Iron Oxide at Room Temperature for Biogas Purification: Application of Renewable Energy. *Renew. Energy* **2020**, *154*, 151-160.

(29) Flores, J. G.; Zárate-Colín, J. A.; Sánchez-González, E.; Valenzuela, J. R.; Gutiérrez-Alejandre, A.; Ramírez, J.; Jancik, V.; Aguilar-Pliego, J.; Zorrilla, M. C.; Lara-García, H. A.; et al. Partially Reversible H_2S Adsorption by MFM-300(Sc): Formation of Polysulfides. *ACS Appl. Mater. Interfaces* **2020**, *12* (16), 18885-18892.

(30) Liu, C.; Zhang, R.; Wei, S.; Wang, J.; Liu, Y.; Li, M.; Liu, R. Selective Removal of H_2S from Biogas Using a Regenerable Hybrid TiO_2/Zeolite Composite. *Fuel* **2015**, *157*, 183-190.

(31) Gupta, N. K.; Bae, J.; Kim, S.; Kim, K. S. Fabrication of Zn-MOF/ZnO Nanocomposites for Room Temperature H_2S Removal: Adsorption, regeneration, and mechanism. *Chemosphere* **2021**, *274*, 129789.

(32) Basina, G.; Gaber, D. A.; Yafei, S. A.; Tzitzios, V.; Gaber, S. A.; Ismail, I.; Vaithilingam, B. V.; Polychronopoulou, K.; Hashimi, S. A.; Wahedi, Y. A. Mesoporous Silica "Plated" Copper Hydroxides/Oxides Heterostructures As Superior Regenerable Sorbents for Low Temperature H_2S Removal. *Chem. Eng. J.* **2020**, *398*, 125585.

(33) Esmaeilnejad, A.; Mahmoudi, P.; Zamanian, A.; Mozafari, M. Synthesis of Titanium Oxide Nanotubes and Their Decoration by Mno Nanoparticles for Biomedical Applications. *Ceram. Int.* **2019**, *45* (15), 19275-19282.

(34) Sánchez-Sánchez, M.; Getachew, N.; Díaz, K.; Díaz-García, M.; Chebude, Y.; Díaz, I. Synthesis of Metal–Organic Frameworks in Water at Room Temperature: Salts As Linker Sources. *Green Chem.* **2015**, *17* (3), 1500-1509.

(35) Reese, B. K.; Finneran, D. W.; Mills, H. J.; Zhu, M.-X.; Morse, J. W. Examination and Refinement of the Determination of Aqueous Hydrogen Sulfide by the Methylene Blue Method. *Aquat. Geochem.* **2011**, *17* (4), 567-582.

(36) Burton, E. D.; Sullivan, L. A.; Bush, R. T.; Johnston, S. G.; Keene, A. F. A Simple and Inexpensive Chromium-Reducible Sulfur Method for Acid-Sulfate Soils. *Appl. Geochem.* **2008**, *23* (9), 2759-2766.

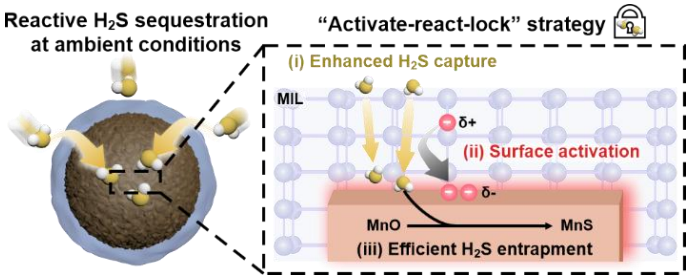
(37) Lee, H. K.; Koh, C. S.; Lo, W.-S.; Liu, Y.; Phang, I. Y.; Sim, H. Y.; Lee, Y. H.; Phan-Quang, G. C.; Han, X.; Tsung, C.-K.; et al. Applying a Nanoparticle@MOF Interface To

Activate an Unconventional Regioselectivity of an Inert Reaction at Ambient Conditions. *J. Am. Chem. Soc.* **2020**, *142* (26), 11521-11527.

(38) Sim, H. Y. F.; Chen, J. R. T.; Koh, C. S. L.; Lee, H. K.; Han, X.; Phan-Quang, G. C.; Pang, J. Y.; Lay, C. L.; Pedireddy, S.; Phang, I. Y.; et al. ZIF-Induced d-Band Modification in a Bimetallic Nanocatalyst: Achieving Over 44 % Efficiency in the Ambient Nitrogen Reduction Reaction. *Angew. Chem. Int. Ed.* **2020**, *59* (39), 16997-17003.

(39) Lu, T.; Chen, F. Multiwfn: A Multifunctional Wavefunction Analyzer. *J. Comput. Chem.* **2012**, *33* (5), 580-592.

TOC Graphic


Reactive H_2S sequestration at ambient conditions
"Activate-react-lock" strategy
(i) Enhanced H_2S capture
MIL
δ+
(ii) Surface activation
δ-
MnO
MnS
(iii) Efficient H_2S entrapment